

# First-principles study of the tensile strength and failure of $\alpha$ -Al<sub>2</sub>O<sub>3</sub>(0001)/Ni(111) interfaces

Siqi Shi,<sup>1,2</sup> Shingo Tanaka,<sup>1</sup> and Masanori Kohyama<sup>1,\*</sup>

<sup>1</sup>Materials Science Research Group, Research Institute for Ubiquitous Energy Devices, National Institute of Advanced Industrial Science and Technology, 1-8-31, Midorigaoka, Ikeda, Osaka 563-8577, Japan

<sup>2</sup>Department of Physics, Center of Optoelectronics Materials and Devices, Zhejiang Sci-Tech University, Xiasha College Park, Hangzhou 310018, China

(Received 18 May 2007; revised manuscript received 21 July 2007; published 29 August 2007)

Tensile strength and failure of Al<sub>2</sub>O<sub>3</sub>(0001)/Ni(111) interfaces have been examined by the first-principles pseudopotential method, and compared with Al<sub>2</sub>O<sub>3</sub>(0001)/Cu(111) interfaces, and effects of the interface stoichiometry, configurations, and metal species have been analyzed. From *rigid-type* tensile tests, the Ni-O interfaces at the O-terminated interfaces are much stronger than the back Ni-Ni interlayers, while the strength of the Ni-Al interfaces at the Al-terminated ones is less than half of the back Ni-Ni interlayers. *Relaxed-type* tensile tests have been applied to the most stable configurations (Al-site and O-site models of the O-terminated and Al-terminated interfaces, respectively) to examine the behavior of atoms and electrons at the failure. For the Al-terminated interface, the Ni-Al interface is naturally broken under lower stress, while catastrophic failure occurs within the interface Ni layer for the O-terminated interface because of the irregular configuration of the interface Ni layer of the Al-site model. Tensile strength and interfacial Young's moduli of Al<sub>2</sub>O<sub>3</sub>/Ni interfaces are larger than those of the Al<sub>2</sub>O<sub>3</sub>/Cu interfaces due to stronger Ni-O and Ni-Al interactions.

DOI: 10.1103/PhysRevB.76.075431

PACS number(s): 68.35.Gy, 68.35.Ct, 82.65.+r, 71.15.Mb

## I. INTRODUCTION

Alumina/metal interfaces are used in various applications, such as coatings, electronic devices, structural composites, electrodes in fuel cells, gas sensors, and heterogeneous catalysis. Such interfaces have a unique electronic structure between two solids with completely different electronic properties, which frequently causes peculiar electronic, chemical, and mechanical properties, as investigated experimentally<sup>1-7</sup> and theoretically.<sup>8-23</sup> Alumina/Cu and alumina/Ni interfaces are especially important in thermal barrier coatings<sup>24</sup> and electronic devices, where the understanding of the adhesive and mechanical properties is crucial. Recent studies have shown that the interface stoichiometry has serious effects on the nature of bonding and properties of alumina/metal interfaces. For Al<sub>2</sub>O<sub>3</sub>(0001)/metal interfaces, O-terminated (O rich), Al-terminated (stoichiometric), and double-Al-layer-terminated (Al rich) interfaces can be constructed by changing the atomic termination of the Al<sub>2</sub>O<sub>3</sub>(0001) surface. The relative stability among the interfaces with different stoichiometries can be determined by free energies including atomic chemical potentials, depending on the oxygen partial pressure or Al activity. For the Al<sub>2</sub>O<sub>3</sub>(0001)/Cu and Al<sub>2</sub>O<sub>3</sub>(0001)/Ni interfaces, *ab initio* thermodynamics analysis<sup>13</sup> indicated that both the Al-terminated (stoichiometric) and O-terminated (O rich) interfaces can exist within the experimental oxygen partial pressure or Al activity.

In our preceding papers,<sup>15-19</sup> we have made detailed analyses on the adhesive and mechanical properties of the O-terminated and Al-terminated Al<sub>2</sub>O<sub>3</sub>(0001)/Cu(111) interfaces by using first-principles calculations based on density-functional theory in collaboration with electron microscopy observations.<sup>6,7</sup> For the O-terminated interfaces, we have observed that strong interfacial Cu-O bonds with both ionic and covalent characters cause much larger adhesive energies than the Al-terminated ones. The presence of Cu 3d-O2p hybrid-

ization and the preference of three-coordinated Cu-O configurations have been confirmed theoretically and experimentally.<sup>7,16,18,19</sup> For the Al-terminated interfaces, the electrostatic (image-charge-like) interaction as well as the Cu-Al hybridization seems to dominate the adhesion. On the mechanical properties, we have applied *ab initio* tensile tests<sup>25,26</sup> to the Al<sub>2</sub>O<sub>3</sub>/Cu interfaces, and observed strong effects of the interface stoichiometry.<sup>17,18</sup> The Cu-O interface at the O-terminated interfaces reveals large strength, resulting in the preferential deformation of Cu regions, although the Cu-Al interface at the Al-terminated ones is initially broken due to the weakness.

Recently, we have examined the nature of bonding and electronic properties of the Al<sub>2</sub>O<sub>3</sub>(0001)/Ni(111) interfaces theoretically using similar atomic models, and observed significant effects of the interface stoichiometry and rigid-body translations (RBTs).<sup>21-23</sup> The adhesion of the O-terminated interfaces is explained by the strong Ni-O bonds with both ionic and covalent characters, and that of the Al-terminated ones is mainly explained by the electrostatic (image-charge-like) and Ni-Al hybridization interactions. However, stronger Ni-O and Ni-Al interactions cause larger adhesive energies and different relative stabilities among the configurations with different RBTs, as compared with the Al<sub>2</sub>O<sub>3</sub>/Cu interfaces.

In this paper, we examine the mechanical properties of the Al<sub>2</sub>O<sub>3</sub>(0001)/Ni(111) interfaces through *ab initio* tensile tests, and discuss the effects of the interface stoichiometry, configurations, and metal species. First, we apply *rigid-type* tensile tests<sup>17,18</sup> so as to clarify the local strength of each Ni-O, Ni-Al, and Ni-Ni interlayer, where the interlayer potential curves are analyzed using the universal binding energy relation (UBER).<sup>27,28</sup> Second, we apply *relaxed-type* tensile tests to the most stable configurations of the O-terminated and Al-terminated interfaces so as to clarify the detailed behavior of atoms and electrons at failure.

## II. THEORETICAL METHOD

Details of the theoretical scheme are already given in Refs. 21–23. We deal with coherent ( $1 \times 1$ )  $\text{Al}_2\text{O}_3(0001)/\text{Ni}(111)$  interfaces with the  $\text{Ni}[1-10]\parallel\text{Al}_2\text{O}_3[1-100]$  relationship. Ni layers are expanded along the interface due to the theoretical lattice misfit of 9.632% (9.488% in experiments<sup>3,29</sup>). We examine three models with different RBTs parallel to the interface, namely, O-site, hollow-site (H-site), and Al-site models, where the interface Ni atom is located above the O, hollow, and Al sites of the hexagonal unit cell of the  $\text{Al}_2\text{O}_3(0001)$  surface, respectively. These correspond to local commensurate regions at an incoherent interface due to the lattice misfit.<sup>14,16</sup> The supercell is constructed by alternate stacking of  $\text{Al}_2\text{O}_3(0001)$  and  $\text{Ni}(111)$  slabs without vacuum regions. The  $\text{Al}_2\text{O}_3$  slab consists of four O atomic layers and eight Al atomic layers, and the top Al layers on both sides are removed for the O-terminated case. The  $\text{Ni}(111)$  slab contains five atomic layers for the O-site and H-site models and seven atomic layers for the Al-site model so as to attain the periodic fcc (111) stacking.

We use the plane-wave pseudopotential method<sup>30</sup> within the local density approximation (LDA).<sup>31</sup> The “residual minimization–direct inversion in the iterative subspace” method<sup>32</sup> is used for the electronic optimization, coupled with an efficient mixing scheme,<sup>33</sup> through the efficiently parallelized code.<sup>34</sup> In each relaxation step, the atomic forces are converged to be less than  $0.05 \text{ eV}/\text{\AA}$ , and the  $C_{3i}$  symmetry of the supercell is preserved. The plane-wave cutoff energy is 120 Ry. Four and nine sampling  $k$  points within the irreducible Brillouin zone of the present supercell are used for self-consistent calculations and for the calculation of local density of states, respectively. For each termination and model, we optimized the RBT normal to the interface, namely, expansion or compression, by iterating the relaxation for various initial values of RBT.

After obtaining relaxed configurations,<sup>21–23</sup> we apply the *ab initio* tensile tests.<sup>17,18</sup> In the rigid-type test, only the selected interface or interlayer is stretched gradually without relaxation. In the relaxed-type test,<sup>25,26</sup> the supercell is stretched in a small increment normal to the interface, atomic positions are changed linearly, and then lattice relaxation is performed. This cycle is iterated until the interface is broken. In this procedure, the cell lengths parallel to the interface are fixed. Thus the present test is not uniaxial tension but uniaxial extension. The present kind of first-principles tensile or shear tests are effective in clarifying the intrinsic strength and local mechanical behavior of materials, as applied to bulk materials or nanowires,<sup>35–37</sup> defected systems,<sup>38,39</sup> and grain boundaries.<sup>25,26,40–44</sup> In contrast, applications to ceramic/metal interfaces are only few.<sup>17,18,45,46</sup>

## III. RESULTS AND DISCUSSION

### A. Rigid-type tensile test

Figure 1(a) shows energy-change curves by the rigid-type tests of the Ni-O interfaces of the O-terminated interfaces as compared with the O-terminated  $\text{Al}_2\text{O}_3/\text{Cu}$  interface.<sup>18</sup> The

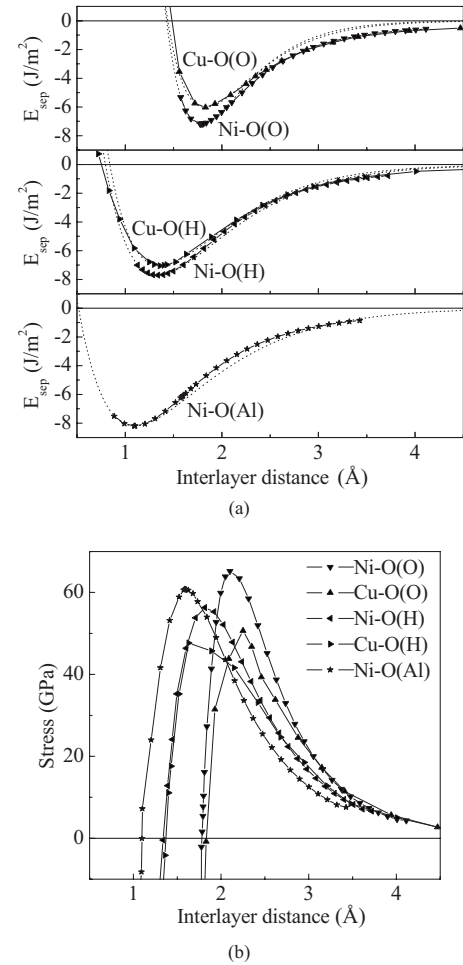


FIG. 1. (a) Interlayer potential curves by the rigid-type tensile test for the Ni-O interlayers of the three models of the O-terminated  $\text{Al}_2\text{O}_3(0001)/\text{Ni}(111)$  interface. (b) Stress vs interlayer distance curves obtained by differentiating the numerical data in (a). Previous results of the O-terminated  $\text{Al}_2\text{O}_3(0001)/\text{Cu}(111)$  interface (H- and O-site models) (Ref. 18) are also plotted. In (a), calculated points are connected by a solid continuous line, while the UBER fitting is shown by a dotted line. The index Ni-O(O) means the Ni-O interface of the O-site model, for example.

energy increase for compression is also calculated. The bottom of each curve corresponds to the separation energy  $E_{sep}$  of the stable configuration, relative to the fixed *separate*  $\text{Al}_2\text{O}_3$  and Ni surfaces.<sup>23</sup> The shapes of the curves for the H-site and Al-site models are rather similar to each other, in spite of different distances of the minimum point, while the shape of the curve of the O-site model is rather different. This is caused by different interfacial configurations. Both the H-site and Al-site models have three-coordinated Ni-O bonds, while the O-site model has dimerlike Ni-O bonds. Thus the curve of the O-site model reveals larger curvature at the bottom and steeper increases against the compression and expansion. Naturally, the local interface Young’s modulus  $Y_I$  obtained from the curvature is the largest for the O-site model, as listed in Table I. A similar phenomenon is observed in the O-site and H-site models of the O-terminated  $\text{Al}_2\text{O}_3/\text{Cu}$  interfaces.<sup>18</sup>

TABLE I. Local interlayer Young's moduli  $Y_I$  of the O-terminated and Al-terminated  $\text{Al}_2\text{O}_3(0001)/\text{Ni}(111)$  interfaces obtained by the rigid-type and relaxed-type tensile tests.  $\bar{Y}$  is the average Young's modulus of the supercell obtained by the relaxed-type test. Previous results of the  $\text{Al}_2\text{O}_3(0001)/\text{Cu}(111)$  interfaces Refs. 17 and 18 are also listed.

	$Y_I$ (GPa) (Rigid)	$Y_I$ (GPa) (Relaxed)	$\bar{Y}$ (GPa) (Relaxed)
$\text{Al}_2\text{O}_3(0001)/\text{Ni}(111)$ interface			
O-term, O-site: Ni-O	403.908		
Ni-Ni	214.938		
H-site: Ni-O	285.573		
Al-site:			239.535
Ni-O	296.871	261.986	
Ni(2)-Ni(1c)	220.479		
Al-term, O-site:			159.446
Ni-Al	66.823	58.797	
Ni-Ni	224.399		
H-site: Ni-Al	41.822		
Al-site: Ni-Al	62.689		
$\text{Al}_2\text{O}_3(0001)/\text{Cu}(111)$ interface			
O-term, O-site:			166
Cu-O	309	225	
H-site:			157
Cu-O	219	145	
Al-term, O-site:			107
Cu-Al	45	38	

The energy curves in Fig. 1(a) are fitted by the UBER function<sup>27,28</sup> expressed as  $E(d) = -E_0(1 + d^*)\exp(-d^*)$ , where  $d^* = (d - d_0)/l$ ,  $l$  is a scaling constant,  $d_0$  is the equilibrium interfacial distance, and  $E_0$  is equal to the separation energy  $E_{sep}$ . Table II lists the values of parameters. The fitting for the Ni-O interfaces is not so successful in Fig. 1(a), similar to the case of the Cu-O interfaces,<sup>18</sup> because the UBER is not suitable for bonds with strong ionic characters or significant charge transfer.

Figure 1(b) shows the tensile stress obtained numerically from the data in Fig. 1(a). The maximum point of each curve, namely, the maximum gradient of each curve in Fig. 1(a), corresponds to the ideal strength of each interlayer,  $\sigma_{max}$ , as summarized in Table II. The strength of the O-site model is the largest, although  $E_{sep}$  is the smallest. As compared with the O-terminated  $\text{Al}_2\text{O}_3/\text{Cu}$  interfaces, the  $\text{Al}_2\text{O}_3/\text{Ni}$  interfaces possess larger tensile strength due to the larger activity of Ni discussed in Refs. 21 and 23.

Figure 2 shows the results of the rigid-type tests of the Ni-Al interfaces of the Al-terminated interfaces as compared with the Al-terminated  $\text{Al}_2\text{O}_3/\text{Cu}$  interface.<sup>17</sup> In Fig. 2(a), the shape of the energy-change curve of the O-site model is similar to that of the Al-site model despite a different distance of the minimum point, while the curve of the H-site

model is much shallower and flatter. In Fig. 2(b) and Table II, the maximum stress is the smallest for the H-site model, while the O-site and Al-site models have similar strength. This relation is also observed in the values of the local interface Young's modulus  $Y_I$  in Table I. As analyzed in Ref. 23, the interfacial bonding is stronger in the O-site and Al-site models than in the H-site model because of the favorable configuration of the O-site model for the electrostatic and Ni-O interactions and because of the favorable configuration of the Al-site model for the Ni-Al hybridization, respectively.

In Fig. 2(a), the UBER fitting is successful for the H-site and Al-site models, while it is worse for the O-site model, different from the same model of the Al-terminated  $\text{Al}_2\text{O}_3/\text{Cu}$  interface.<sup>17</sup> This can be explained by the special nature of bonding of the O-site model of the Al-terminated  $\text{Al}_2\text{O}_3/\text{Ni}$  interface containing the Ni-O hybridization,<sup>23</sup> which is not observed in the other models of the Al-terminated  $\text{Al}_2\text{O}_3/\text{Ni}$  interface; the Cu-O hybridization was also not observed in the Al-terminated  $\text{Al}_2\text{O}_3/\text{Cu}$  interface.<sup>17</sup>

Figure 3 shows the results of the rigid-type tests for the back Ni-Ni interlayers of three kinds of  $\text{Al}_2\text{O}_3/\text{Ni}$  interfaces as denoted by Ni(2)-Ni(1)(O), Ni(2)-Ni(1c), and Ni(2)-Ni(1). The energy and stress curves have shapes similar to each other, resulting in similar values of  $E_{sep}$ ,  $Y_I$ , and  $\sigma_{max}$  in Tables I and II, in spite of the different termination and RBT of the three interfaces. This indicates that the back Ni-Ni bonds suffer from only small effects of the interface configuration by metallic screening as observed in the  $\text{Al}_2\text{O}_3/\text{Cu}$  interfaces.<sup>17,18</sup> The UBER fitting is successful for these three curves due to the metallic nature, similar to the Cu-Cu interlayers. The energy and tensile strength for the Ni-Ni interlayer are intervening between those for the Ni-O and Ni-Al interlayers, and those for the Ni-Ni interlayer are larger than those for the Cu-Cu interlayer due to the stronger bulk Ni bonding caused by its electronic structure. Here, the present value of  $E_{sep}$  for the back Ni-Ni interlayer is somewhat larger than that (4.08 J/m<sup>2</sup>) for the back Ni-Ni interlayer at the  $\text{ZrO}_2/\text{Ni}(111)$  interface.<sup>46</sup> This should be caused by the usage of the generalized gradient approximation in Ref. 46, and the LDA somewhat overestimates surface energies as analyzed in our papers.<sup>15,21,23</sup> Note that the present tensile strength of the back Ni-Ni interlayer is close to the experimental tensile strength of bulk Ni along the [100] direction [37 GPa (Ref. 47)].

In the Al-site model of the O-terminated interface, the three Ni atoms of the interface Ni layer in the unit cell have slightly different heights by the symmetry, and the rigid-type tests have been applied additionally to the cleavage at the three sublayers Ni(1a), Ni(1b), and Ni(1c), as shown in Fig. 3. The stable Ni-O interlayer distances (bond lengths) between Ni(1a), Ni(1b), Ni(1c), and O layers are 1.097 Å (2.008 Å), 1.366 Å (2.018 Å), and 1.585 Å (2.217 Å), respectively. The Ni(1a) atom is located on the center of an O triangle, where the surface Al atom exists in the stoichiometric surface. The Ni(1b) atom is located on the center of another O triangle just above the subsurface Al(3) atom, and the Ni(1c) atom is also located on the center of another O triangle just above the subsurface Al(2) atom. As listed in Table II, values of  $E_{sep}$  for the Ni(1b)-Ni(1a), Ni(1c)-Ni(1b), and Ni(2)-Ni(1c) interlayers are 5.851, 5.419, and

TABLE II. UBER fitting parameters,  $d_0$ ,  $l$ , and  $E_0$  ( $E_{sep}$ ), and tensile strength  $\sigma_{max}$  of the O-terminated and Al-terminated  $\text{Al}_2\text{O}_3(0001)/\text{Ni}(111)$  interfaces. Previous results of the  $\text{Al}_2\text{O}_3(0001)/\text{Cu}(111)$  interface Refs. 17 and 18 are also listed.

	$d_0$ (Å)	$l$ (Å)	$E_0$ (J/m <sup>2</sup> )	$\sigma_{max}$ (GPa) (Rigid)	$\sigma_{max}$ (GPa) (Relaxed)
$\text{Al}_2\text{O}_3(0001)/\text{Ni}(111)$ interface					
O-term, O-site: Ni-O	1.785	0.357	7.178	64.100	
Ni-Ni	1.816	0.595	5.519	36.313	
H-site: Ni-O	1.338	0.544	7.713	56.311	
Al-site:					28.301
Ni-O	1.097	0.582	8.193	61.003	
Ni(1b)-Ni(1a)			5.851	36.530	
Ni(1c)-Ni(1b)			5.419	27.598	
Ni(2)-Ni(1c)	1.546	0.602	5.422	35.086	
Al-term, O-site:					15.384
Ni-Al	1.609	0.455	2.387	16.832	
Ni-Ni	1.848	0.597	5.455	36.029	
H-site: Ni-Al	1.989	0.534	1.262	8.743	
Al-site: Ni-Al	2.282	0.536	2.430	16.437	
$\text{Al}_2\text{O}_3(0001)/\text{Cu}(111)$ interface					
O-term, O-site: Cu-O	1.83	0.39	6.04	46.2	
Cu-Cu				25.1	
H-site: Cu-O	1.36	0.52	7.07	49.9	
Cu-Cu	1.93	0.52	3.74	25.9	
Al-term, O-site:					10.1
Cu-Al	1.83	0.49	1.62	12.1	
Cu-Cu			3.71	25.4	

5.422 J/m<sup>2</sup>, respectively, and the values of the ideal strength are 36.530, 27.598, and 35.086 GPa, respectively. The separation energy and ideal strength are the smallest for the Ni(1c)-Ni(1b) interlayer, which indicates the possible initiation of tensile failure at this position as will be examined in the relaxed-type test. The reason of the weakness of the Ni(1c)-Ni(1b) interlayer seems to be the much larger Ni(1c)-O bond length than the Ni(1b)-O and Ni(1a)-O bond lengths as will be analyzed later. The UBER fitting for the Ni(1b)-Ni(1a) and Ni(1c)-Ni(1b) interlayers is not successful, which should be caused by the complex mixture of Ni-Ni and Ni-O interactions.

## B. Relaxed-type tensile test

### 1. Interface Young's modulus

Relaxed-type tensile tests have been applied to the most stable configuration of each interface stoichiometry, namely, the Al-site model of the O-terminated interface and the O-site model of the Al-terminated interface. By the relaxed-type tests, we can analyze the interface Young's modulus.<sup>17,18</sup> First, an average Young's modulus  $\bar{Y}$  for each supercell is

obtained through the relaxed-type test in the region of small strains as listed in Table I. The value of the O-terminated interface is larger than the experimental Young's modulus of bulk Ni [201.5 GPa (Ref. 48)] and smaller than that of bulk  $\text{Al}_2\text{O}_3$  [345 GPa (Ref. 49)], whereas the value of the Al-terminated interface is much smaller than both the bulk values. Then we obtain the local interface Young's modulus  $Y_I$  using the relation of  $(1/\bar{Y}) = (R_I/Y_I) + (R_{\text{Ni}}/Y_{\text{Ni}}) + (R_{\text{Al}_2\text{O}_3}/Y_{\text{Al}_2\text{O}_3})$ , where  $Y_{\text{Ni}}$  and  $Y_{\text{Al}_2\text{O}_3}$  are the Young's moduli of Ni and  $\text{Al}_2\text{O}_3$  along the [111] and [0001] directions, respectively, and  $R_I$ ,  $R_{\text{Ni}}$ , and  $R_{\text{Al}_2\text{O}_3}$  are the ratio of the length of each region in the direction normal to the interface against the cell length. Using the experimental values of bulk Ni and  $\text{Al}_2\text{O}_3$  for  $Y_{\text{Al}_2\text{O}_3}$  and  $Y_{\text{Ni}}$ , we obtain  $Y_I$  of 261.986 GPa for the Al-site model of the O-terminated interface and  $Y_I$  of 58.797 GPa for the O-site model of the Al-terminated interface. These values are smaller than those from the interlayer curves by the rigid-type tests (296.871 and 66.823 GPa), while these are more correct by including the effects of relaxation. It is natural that these are larger than the values of the  $\text{Al}_2\text{O}_3/\text{Cu}$  interfaces as listed in Table I, due to the stronger Ni-O and Ni-Al interactions.<sup>23</sup>

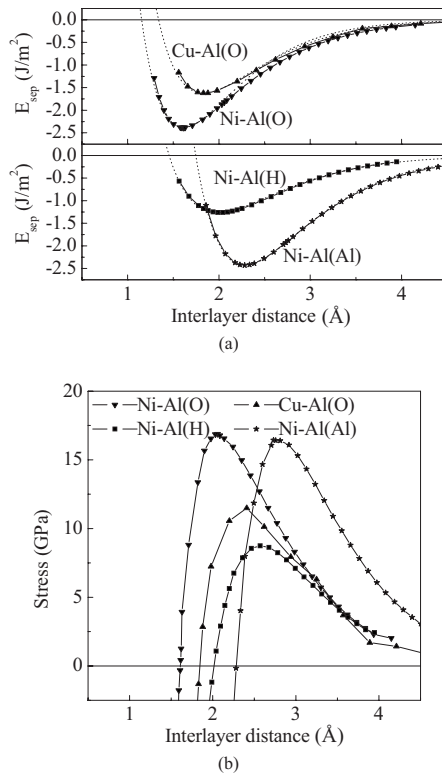


FIG. 2. (a) Interlayer potential curves by the rigid-type tensile test for the Ni-Al interlayers of the three models of the Al-terminated  $\text{Al}_2\text{O}_3(0001)/\text{Ni}(111)$  interface. (b) Stress vs interlayer distance curves obtained by differentiating the numerical data in (a). Previous result of the Al-terminated  $\text{Al}_2\text{O}_3(0001)/\text{Cu}(111)$  interface (O-site model) (Ref. 17) is also plotted. In (a), calculated points are connected by a solid continuous line, while the UBER fitting is shown by a dotted line.

## 2. Al-site model of the O-terminated interface

Figure 4 shows the energy-strain and stress-strain curves by the relaxed-type tensile test of the Al-site model of the O-terminated interface. Curves of the rigid-type tests for the cleavage between the Ni sublayers are also plotted, where the tensile strain is defined by the total cell length containing the rigid increase of the interlayer distance. The energy curve of the relaxed-type test is lower than the other curves by lattice relaxation for the same cell length (strain). The stress reaches the maximum of 28.301 GPa at the strain of 14.0% in the relaxed-type test, where the stretching at the maximum point is larger than the other curves due to the relaxation. The maximum stress in the relaxed-type test is close to the strength of the Ni(1c)-Ni(1b) interlayer by the rigid-type test (27.598 GPa), and indeed, the failure occurs at this interlayer. The stress drops suddenly after the strain of 14%. This catastrophic feature is quite different from the continuous change for the Al-terminated interface, which will be described later.

Figure 5(a) shows the changes in each interlayer distance during the relaxed-type test, where the vertical line represents the strain of the maximum stress. Before the strain of 6%, all the interlayer distances increase naturally according

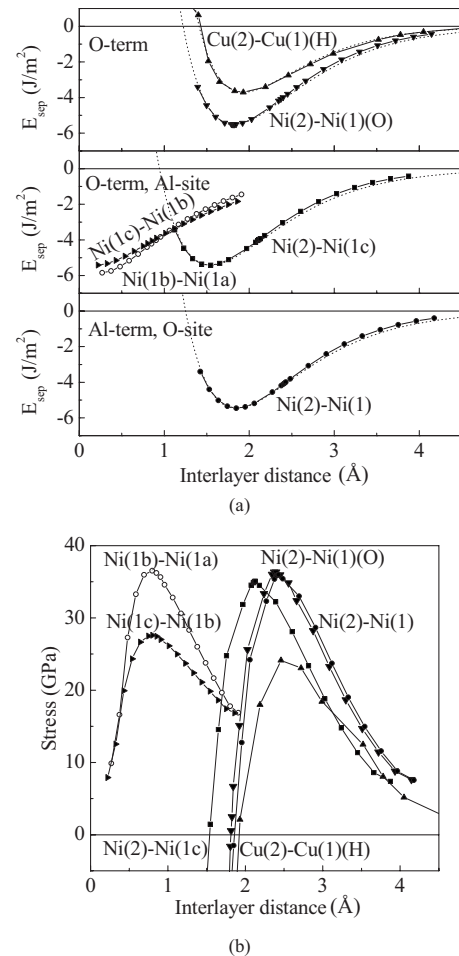


FIG. 3. (a) Interlayer potential curves by the rigid-type tensile test for the Ni-Ni interlayers of the O-terminated  $\text{Al}_2\text{O}_3(0001)/\text{Ni}(111)$  interface (O- and Al-site models) and the Al-terminated  $\text{Al}_2\text{O}_3(0001)/\text{Ni}(111)$  interface (O-site model). (b) Stress vs interlayer distance curves obtained by differentiating the numerical data in (a). Previous results of the O-terminated  $\text{Al}_2\text{O}_3(0001)/\text{Cu}(111)$  interface (H-site model) (Ref. 18) are also plotted. In (a), calculated points are connected by a solid continuous line, while the UBER fitting is shown by a dotted line. The indices Ni(1) and Ni(2) mean the interface Ni and back (second) Ni layers. Ni(1a), Ni(1b), and Ni(1c) mean the three Ni sublayers of the interface Ni layer of the Al-site model of the O-terminated interface.

to the elastic property of each region, except for the peculiar behavior of the Al(2)-Al(3) interlayer. The stretching is relatively larger in the region from the interface O layer to the Ni(2) layer containing the three Ni sublayers. After the strain of 6%, the Ni(1a)-O(1) interlayer begins to shrink, resulting in the increase of the Ni(1a)-Ni(1b) and Ni(1a)-Ni(1c) interlayer distances. After the strain of 10%, the increase of the Ni(1c)-O(1) interlayer distance is larger than that of the Ni(1b)-O(1) interlayer distance, resulting in the increase of the Ni(1c)-Ni(1b) interlayer distance. After the strain of 14%, the Ni(1b)-O(1) interlayer distance begins to shrink, resulting in the clear failure at the Ni(1c)-Ni(1b) interlayer after the strain of 15%.

About the bond-length changes shown in Fig. 5(b), it is interesting that the Ni(1c)-O(1) bond length is quite larger

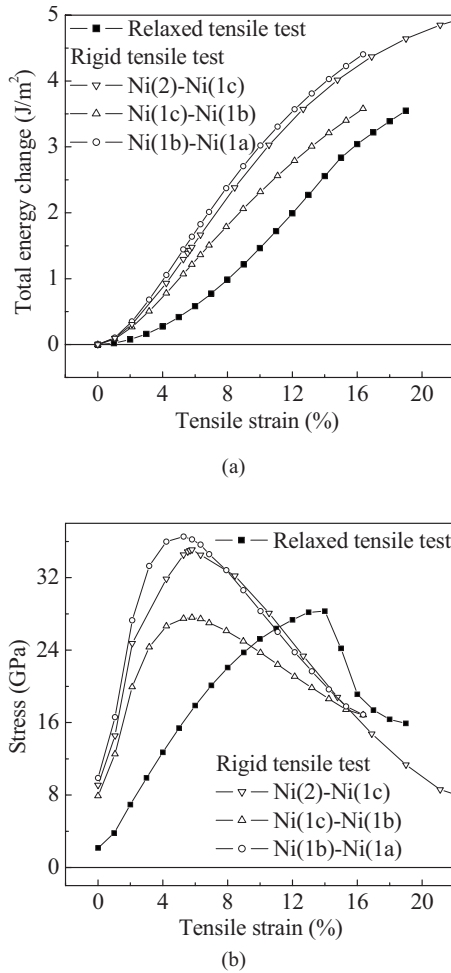


FIG. 4. (a) Energy-strain and (b) stress-strain curves of the Al-site model of the O-terminated  $\text{Al}_2\text{O}_3(0001)/\text{Ni}(111)$  interface in the relaxed-type tensile test compared with those of the Ni(1b)-Ni(1a), Ni(1c)-Ni(1b), and Ni(2)-Ni(1c) interlayers by the rigid-type tensile test.

than the other Ni-O bonds in the initial configuration. After the strain of 6%, Ni(1a)-O(1) bond length begins to shrink, resulting in the increases of the Ni(1a)-Ni(2) and Ni(1a)-Ni(1c) bond lengths. After the strain of 10%, the increase of the Ni(1c)-O(1) bond length becomes larger than that of the Ni(1b)-O(1) bond length, and similarly, the increase of the Ni(1b)-Ni(2) bond length becomes larger than that of the Ni(1c)-Ni(2) bond length. After the strain of 14%, the Ni(1b)-O(1) bond length begins to shrink, and the Ni(1c)-O(1) bond length reveals rapid increase. Then after the strain of 15%, the in-plane bond breaking occurs at the Ni(1b)-Ni(1c) and Ni(1a)-Ni(1c) bonds, as well as the breaking of the Ni(1c)-O(1), Ni(1a)-Ni(2), and Ni(1b)-Ni(2) bonds.

Figure 6 shows the evolution of the valence charge density distribution at the failure in the relaxed-type tensile test. To analyze the features of Ni-O hybridization, we plot the charges around the Ni-O bonds only from eigenstates in selected energy regions, corresponding to the range of the lower part of the oxygen upper valence band and the bottom of the Ni 3d band, including the 4s band. In the stable configuration, the Ni(1a)-O and Ni(1b)-O bonds in Figs. 6(a)

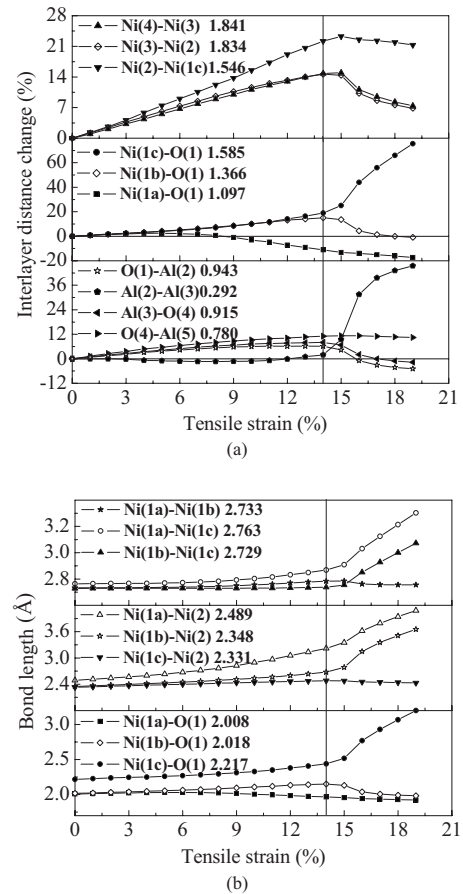


FIG. 5. Variation in (a) interlayer distances and (b) interfacial Ni-O, back Ni-Ni, and in-plane Ni-Ni bond lengths during the relaxed-type tensile test of the Al-site model of the O-terminated  $\text{Al}_2\text{O}_3(0001)/\text{Ni}(111)$  interface. Values of interlayer distances and bond lengths at the stable configuration are listed inside each panel in units of Å. The layer index  $M(n)$  means the  $n$ th layer of element  $M$  from the interface. Ni(1a), Ni(1b), and Ni(1c) mean the three Ni sublayers of the interface Ni layer. The vertical line indicates the strain of the maximum stress.

and 6(b) seem to be strong with enough hybridization charge and shorter bond lengths (2.008 and 2.018 Å) as compared with the Ni(1c)-O bond in Fig. 6(c) with less hybridization charge and longer bond length (2.217 Å).

At the strain of 14% shown in Figs. 6(d)–6(f), the stretchings of the Ni(1a)-O, Ni(1b)-O, and Ni(1c)-O bond lengths are  $-2.032\%$ ,  $6.547\%$ , and  $9.950\%$ , respectively, as compared with those of the stable configuration. The stretchings of the Ni(1b)-Ni(1a), Ni(1c)-Ni(1b), and Ni(2)-Ni(1c) interlayer distances are  $121.760\%$ ,  $43.511\%$ , and  $22.188\%$ , respectively. From the hybridization charge, it is clear that the Ni(b)-O and Ni(1c)-O bonds are weakened, while the Ni(1a)-O bond is strengthened. The decrease of the charge is remarkable at the Ni(1c)-O bond.

At the strain of 16% shown in Figs. 6(g)–6(i), the stretchings of the Ni(1a)-O, Ni(1b)-O, and Ni(1c)-O bond lengths are  $-3.217\%$ ,  $0.966\%$ , and  $24.886\%$ , respectively. It is clear that the hybridization charge is increased at the Ni(1b)-O bond due to the bond-length recovery. The respective stretch-

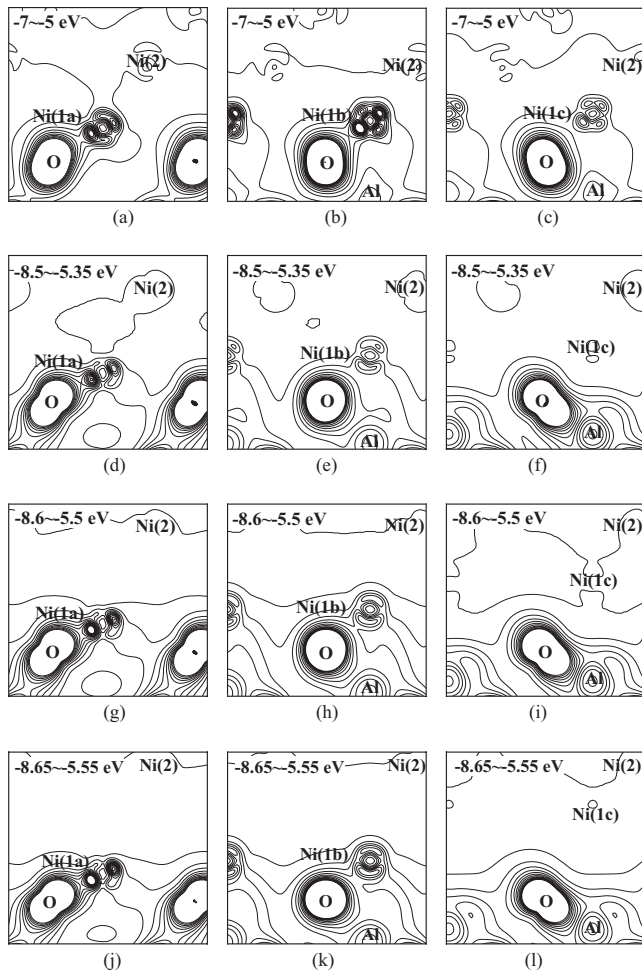


FIG. 6. Charge density distributions around the Ni-O bonds of the Al-site model of the O-terminated  $\text{Al}_2\text{O}_3(0001)/\text{Ni}(111)$  interface for different tensile strains of (a)–(c) 0%, (d)–(f) 14%, (g)–(i) 16%, and (j)–(l) 19% in the relaxed-type tensile test. Hybridization charges from eigenstates in the selected energy window are plotted. Contours are plotted from 0.0005 to 0.0125 a.u. $^{-3}$  with a spacing of 0.0012 a.u. $^{-3}$ .

ings of the Ni(1b)-Ni(1a), Ni(1c)-Ni(1b), and Ni(2)-Ni(1c) interlayer distances are 79.537%, 290.492%, and 22.555%. The Ni(1c)-Ni(1b) interlayer shows rapid expansion in contrast to the shrinkage of the Ni(1b)-Ni(1a) interlayer, which means that the failure has occurred at the Ni(1c)-Ni(1b) interlayer. After this failure, the Ni slab above the Ni(1c) layer and the  $\text{Al}_2\text{O}_3$  slab with the Ni(1b) and Ni(1a) sublayers shrink. At the strain of 19% shown in Figs. 6(j)–6(l), the total compressions of the two slabs and the expansion of the Ni(1c)-Ni(1b) interlayer are 4.799%, 6.392%, and 354.070% against those at the strain of 14%, respectively.

In Fig. 5(a), we can see the marked increase of the Al(2)-Al(3) interlayer distance within the  $\text{Al}_2\text{O}_3$  slab after the failure. This change seems to be correlated with the behavior of the Ni(1c) and Ni(1b) layers. In Figs. 6(f), 6(i), and 6(l), the Al(2) atom is visible below the O(1) atom, with the same coordinates on the (0001) plane as the Ni(1c) atom. The Al(2) atom goes up according to the moving away of the Ni(1c) atom at the failure. Similarly, the Al(3) atom is visible

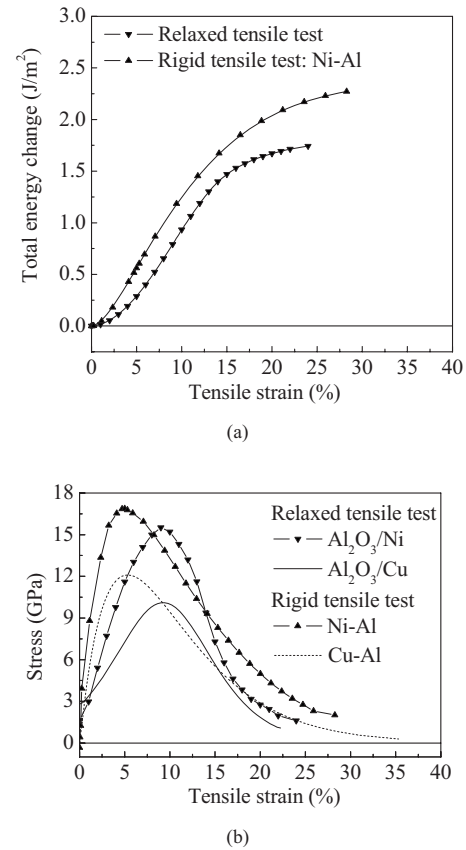


FIG. 7. (a) Energy-strain and (b) stress-strain curves of the O-site model of the Al-terminated  $\text{Al}_2\text{O}_3(0001)/\text{Ni}(111)$  interface by the relaxed-type tensile test compared with those by the rigid-type tensile test. Previous results of the O-site model of the Al-terminated  $\text{Al}_2\text{O}_3(0001)/\text{Cu}(111)$  interface (Ref. 17) are also plotted.

in Figs. 6(e), 6(h), and 6(k), and it goes down according to the sink of the Ni(1b) atom. The nature of the  $\text{Al}_2\text{O}_3$  surface with the two Ni sublayers remaining is quite different from the interface or clean surface, which seems to cause the peculiar behavior of the subsurface Al atoms.

### 3. O-site model of the Al-terminated interface

Figure 7 shows the energy-strain and stress-strain curves by the relaxed-type tensile test of the O-site model of the Al-terminated interface, as well as similar curves by the rigid-type test for the Ni-Al interlayer of the same model, where the tensile strain is defined by the total cell length. It is natural that the energy curve by the relaxed-type test is lower by lattice relaxation, and that the stress curve by the relaxed-type test reveals the lower maximum stress (15.384 GPa) at the longer critical strain (9.181%), as compared with the value of 16.832 GPa at 4.982% in the rigid-type test. The Ni-Al interlayer distance at the strain of 9% is 2.158 Å, which is rather similar to that of 2.059 Å at 4.982% in the rigid-type test. The stress drops rather continuously after the maximum, which is different from the O-terminated interface [Fig. 4(b)]. This feature is similar to the curve of the same model of the  $\text{Al}_2\text{O}_3/\text{Cu}$  interface,<sup>17</sup> where the maximum



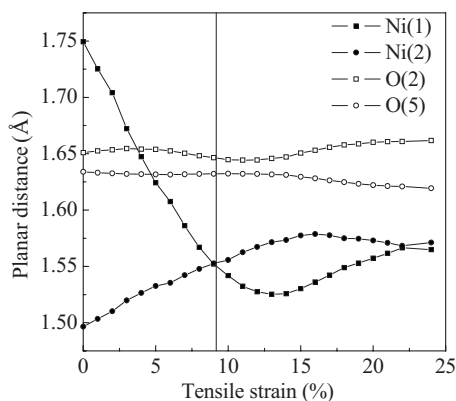


FIG. 10. Variation in the in-plane distance between each atom and the projected position of the Al(1) atom on each layer during the relaxed-type tensile test of the O-site model of the Al-terminated  $\text{Al}_2\text{O}_3(0001)/\text{Ni}(111)$  interface.

changed due to the symmetry. The projected position of the interface Ni atom obviously moves toward the interface Al atom during the tensile process even after the maximum stress so as to maintain the Ni-Al interactions, and after the failure, it recovers. This causes the displacements of the other Ni and O atoms. The magnitude of the in-plane displacement of the interface Ni atom is larger by 50% than that in the  $\text{Al}_2\text{O}_3/\text{Cu}$  interface, indicating stronger Ni-Al interactions.

### C. Discussion

The mechanical properties of each interface obtained by the rigid-type tensile tests are consistent with the nature of bonding of each interface examined in Ref. 23. The O-terminated interfaces with ionic and covalent Ni-O bonds have quite larger strength and Young's moduli than the Al-terminated interfaces with weak electrostatic and hybridization interactions. For each interface stoichiometry, the three kinds of configurations reveal substantially different mechanical properties according to each nature of bonding. The UBER fitting of the interlayer potential curve has been shown to be a good measure to examine the nature of bonding as observed in the  $\text{Al}_2\text{O}_3/\text{Cu}$  interfaces.<sup>17,18</sup> The ideal strength and interface Young's moduli of the  $\text{Al}_2\text{O}_3/\text{Ni}$  interfaces are, indeed, larger than those of the  $\text{Al}_2\text{O}_3/\text{Cu}$  interfaces, due to the higher activity of Ni as discussed in Ref. 23.

It is interesting that the results of the relaxed-type tests are consistent with those of the rigid-type tests. For the Al-terminated interface (O-site model), the Ni-Al interface is naturally broken in the relaxed-type test for the critical Ni-Al interlayer stretching (2.158 Å), similar to that in the rigid-type test (2.059 Å). For the O-terminated interface (Al-site model), the failure occurs at the Ni(1c)-Ni(1b) interlayer in the relaxed-type test for the critical stress (28.301 GPa), rather similar to the ideal strength of the Ni(1c)-Ni(1b) interlayer by the rigid-type test (27.598 GPa), and this interlayer is the weakest in the rigid-type tests. All these results may be caused by rather simple configurations of the present interfaces with only few independent atoms in each layer.

It should be noted that the *ab initio* tensile tests are essential to understand the interface mechanical properties. Only the adhesive or separation energies obtained in Ref. 23 do not provide enough information. The O-site model has the largest ideal strength and Young's modulus in the O-terminated  $\text{Al}_2\text{O}_3/\text{Ni}$  interfaces in spite of the smallest separation and adhesion energies. Detailed features of the failure process can be revealed only by the relaxed-type tests according to the natural behavior of atoms and electrons. The present in-plane failure of the interface Ni layer of the Al-site model of the O-terminated interface is revealed by virtue of this test, where the Ni 3d-O 2p hybridization is shown to dominate the interface strength and the in-plane failure.

From the present results, the strength and failure should firstly depend on the interface stoichiometry, indicating the importance of the control of the atmosphere in the interface formation. The Al-terminated interfaces are rather weak and the failure occurs at the Ni-Al interface, resulting in lower toughness. The O-terminated interfaces have much higher strength, and the failure should occur in the Ni side at least, resulting in larger toughness. Secondly, the strength and failure process should depend on the features of configurations such as coordination and irregularity of the interface plane, as shown in the in-plane failure of the Al-site model of the O-terminated interface. This kind of complex failure should also contribute to the increase of the toughness. Of course, real experimental interfaces with the lattice misfit should contain various configurations with different RBTs as well as more disordered configurations, defects, or impurities, which should cause more complex features of failure. There have been few experimental studies on the mechanical properties of  $\text{Al}_2\text{O}_3/\text{Ni}$  interfaces at the atomic scale, although the present results should be useful to make a detailed analysis of experimental results in the future.

Finally, we would like to emphasize that the interlayer potential curves in Figs. 1(a), 2(a), and 3(a) as well as the results of the relaxed-type tests and stable configurations are useful for the construction of effective interatomic potentials as recently performed for the  $\text{Al}_2\text{O}_3/\text{Cu}$  system,<sup>50-52</sup> which is one of the practical schemes to link *ab initio* calculations and large-scale simulations. This is a challenge because of the absence of simple models of oxide/metal interfacial bonding with specific functional forms. Due to the completely different nature of bonding for the O-terminated and Al-terminated interfaces, two sets of potentials should be determined and selected according to the local interface stoichiometry.<sup>52</sup> The key problem is multidimensional optimization of interatomic potentials so as to reproduce various *ab initio* results.

### IV. SUMMARY

We have investigated the tensile strength and failure process of the  $\alpha\text{-Al}_2\text{O}_3(0001)/\text{Ni}(111)$  interfaces by the first-principles calculations, and made the comparison with the  $\text{Al}_2\text{O}_3(0001)/\text{Cu}(111)$  interfaces. We have observed that the interface stoichiometry as well as the configuration have significant effects on the tensile strength and fracture. The rigid-type tensile tests have clarified ideal local strength and local

Young's moduli of each Ni-O, Ni-Al, and Ni-Ni interlayer, for which the interlayer potential curves are analyzed by the UBER fitting. The Ni-O and Ni-Al interfaces are nearly twice stronger and weaker than that of the back Ni-Ni interlayer, respectively. The relaxed-type tests have been applied to the most stable configuration of each interface stoichiometry. The Ni-Al interface is broken naturally under lower stress at the Al-terminated interface (O-site model), although catastrophic failure occurs within the interface Ni layer of the O-terminated interface (Al-site model) due to the irregular configuration of the interface Ni layer. It has been clearly shown that the behavior of valence electrons really dominates the strength and failure process. The tensile strength

and interfacial Young's modulus of  $\text{Al}_2\text{O}_3(0001)/\text{Ni}(111)$  interfaces are larger than those of the  $\text{Al}_2\text{O}_3(0001)/\text{Cu}(111)$  interfaces due to the larger activity of Ni.

#### ACKNOWLEDGMENTS

The present work was supported by the New Energy and Industrial Development Organization (NEDO) as the Nano-Coating Project. The authors would like to thank R. Yang, S. Dmitriev, W. Zhang, N. Yoshikawa, Y. Hangai, and Y. Kagawa for fruitful discussions. All the computations were performed on the HITACHI SR11000 supercomputer at the Tsukuba Advanced Computing Center (TACC), AIST.

\*Corresponding author; m-kohyama@aist.go.jp

- <sup>1</sup>D. Chatain, L. Coudurier, and N. Eustathopoulos, *Rev. Phys. Appl.* **23**, 1055 (1988).
- <sup>2</sup>F. S. Ohuchi and M. Kohyama, *J. Am. Ceram. Soc.* **74**, 1163 (1991).
- <sup>3</sup>G. Dehm, M. Rühle, G. Ding, and R. Raj, *Philos. Mag. B* **71**, 1111 (1995).
- <sup>4</sup>E. Saiz, R. M. Cannon, and A. P. Tomsia, *Acta Mater.* **47**, 4209 (1999).
- <sup>5</sup>C. Scheu, M. Gao, and M. Rühle, *J. Mater. Sci. Technol.* **18**, 117 (2002).
- <sup>6</sup>T. Sasaki, K. Matsunaga, H. Ohta, H. Hosono, T. Yamamoto, and Y. Ikuhara, *Sci. Technol. Adv. Mater.* **4**, 575 (2003).
- <sup>7</sup>T. Sasaki, T. Mizoguchi, K. Matsunaga, S. Tanaka, T. Yamamoto, M. Kohyama, and Y. Ikuhara, *Appl. Surf. Sci.* **241**, 87 (2005).
- <sup>8</sup>M. W. Finnis, *J. Phys.: Condens. Matter* **8**, 5811 (1996).
- <sup>9</sup>I. G. Batirev, A. Alavi, M. W. Finnis, and T. Deutsch, *Phys. Rev. Lett.* **82**, 1510 (1999).
- <sup>10</sup>W. Zhang and J. R. Smith, *Phys. Rev. B* **61**, 16883 (2000).
- <sup>11</sup>W. Zhang and J. R. Smith, *Phys. Rev. Lett.* **85**, 3225 (2000).
- <sup>12</sup>I. G. Batyrev and L. Kleinman, *Phys. Rev. B* **64**, 033410 (2001).
- <sup>13</sup>W. Zhang, J. R. Smith, and A. G. Evans, *Acta Mater.* **50**, 3803 (2002).
- <sup>14</sup>W. Zhang, J. R. Smith, X.-G. Wang, and A. G. Evans, *Phys. Rev. B* **67**, 245414 (2003).
- <sup>15</sup>R. Yang, S. Tanaka, and M. Kohyama, *Philos. Mag. Lett.* **84**, 425 (2004).
- <sup>16</sup>S. Tanaka, R. Yang, M. Kohyama, T. Sasaki, K. Matsunaga, and Y. Ikuhara, *Mater. Trans.* **45**, 1973 (2004).
- <sup>17</sup>R. Yang, S. Tanaka, and M. Kohyama, *Philos. Mag.* **85**, 2961 (2005).
- <sup>18</sup>S. Tanaka, R. Yang, and M. Kohyama, *Philos. Mag.* **86**, 5123 (2006).
- <sup>19</sup>T. Mizoguchi, T. Sasaki, S. Tanaka, K. Matsunaga, T. Yamamoto, M. Kohyama, and Y. Ikuhara, *Phys. Rev. B* **74**, 235408 (2006).
- <sup>20</sup>A. Hashibon, C. Elsässer, and M. Rühle, *Acta Mater.* **53**, 5323 (2005).
- <sup>21</sup>S. Q. Shi, S. Tanaka, and M. Kohyama, *Modell. Simul. Mater. Sci. Eng.* **14**, S21 (2006).
- <sup>22</sup>S. Q. Shi, S. Tanaka, and M. Kohyama, *Mater. Trans.* **47**, 2696 (2006).
- <sup>23</sup>S. Q. Shi, S. Tanaka, and M. Kohyama, *J. Am. Ceram. Soc.* **90**, 2429 (2007).
- <sup>24</sup>A. G. Evans, D. R. Mumm, J. W. Hutchinson, G. H. Meier, and F. S. Petit, *Prog. Mater. Sci.* **46**, 505 (2001).
- <sup>25</sup>M. Kohyama, *Philos. Mag. Lett.* **79**, 659 (1999).
- <sup>26</sup>M. Kohyama, *Phys. Rev. B* **65**, 184107 (2002).
- <sup>27</sup>J. H. Rose, J. R. Smith, and J. Ferrante, *Phys. Rev. B* **28**, 1835 (1983).
- <sup>28</sup>A. Banerjee and J. R. Smith, *Phys. Rev. B* **37**, 6632 (1988).
- <sup>29</sup>C. Kittel, *Introduction to Solid State Physics*, 6th ed. (Wiley, New York, 1986).
- <sup>30</sup>N. Troullier and J. L. Martins, *Phys. Rev. B* **43**, 1993 (1991).
- <sup>31</sup>J. P. Perdew and A. Zunger, *Phys. Rev. B* **23**, 5048 (1981).
- <sup>32</sup>G. Kresse and J. Furthmüller, *Phys. Rev. B* **54**, 11169 (1996).
- <sup>33</sup>P. Pulay, *J. Comput. Chem.* **3**, 556 (1982).
- <sup>34</sup>T. Tamura, G.-H. Lu, R. Yamamoto, M. Kohyama, S. Tanaka, and Y. Tateizumi, *Modell. Simul. Mater. Sci. Eng.* **12**, 945 (2004).
- <sup>35</sup>Y. M. Huang, J. C. H. Spence, and O. F. Sankey, *Philos. Mag. A* **70**, 53 (1994).
- <sup>36</sup>M. Šob, M. Friák, D. Legut, J. Fiala, and V. Vitek, *Mater. Sci. Eng., A* **387-389**, 148 (2004), and references therein.
- <sup>37</sup>K. S. Chan, Y. D. Lee, and Y. M. Pan, *Metall. Mater. Trans. A* **37A**, 523 (2006).
- <sup>38</sup>V. B. Deyirmenjian, V. Heine, M. C. Payne, V. Milman, R. M. Lynden-Bell, and M. W. Finnis, *Phys. Rev. B* **52**, 15191 (1995).
- <sup>39</sup>R. Pérez and P. Gumbsch, *Phys. Rev. Lett.* **84**, 5347 (2000).
- <sup>40</sup>C. Molteni, G. P. Francis, M. C. Payne, and V. Heine, *Phys. Rev. Lett.* **76**, 1284 (1996).
- <sup>41</sup>C. Molteni, N. Marzari, M. C. Payne, and V. Heine, *Phys. Rev. Lett.* **79**, 869 (1997).
- <sup>42</sup>G.-H. Lu, S. Deng, T. Wang, M. Kohyama, and R. Yamamoto, *Phys. Rev. B* **69**, 134106 (2004).
- <sup>43</sup>G.-H. Lu, Y. Zhang, S. Deng, T. Wang, M. Kohyama, R. Yamamoto, F. Liu, K. Horikawa, and M. Kanno, *Phys. Rev. B* **73**, 224115 (2006).
- <sup>44</sup>M. Yamaguchi, M. Shiga, and H. Kaburaki, *Science* **307**, 393 (2005).
- <sup>45</sup>S. Ogata and H. Kitagawa, *J. Jpn. Inst. Met.* **60**, 1079 (1996).
- <sup>46</sup>K. Matsunaga, T. Sasaki, N. Shibata, T. Mizoguchi, T. Yamamoto, and Y. Ikuhara, *Phys. Rev. B* **74**, 125423 (2006).
- <sup>47</sup>A. Kelly and N. H. Macmillan, *Strong Solids*, 3rd ed. (Clarendon, Oxford, 1986).
- <sup>48</sup>J. A. Ruud, D. Josell, and F. Spaepen, *J. Mater. Res.* **8**, 112

- (1993).
- <sup>49</sup>J. F. Shackelford and W. Alexander, *CRC Materials Science and Engineering Handbook* (CRC, Boca Ration, FL, 2001).
- <sup>50</sup>S. V. Dmitriev, N. Yoshikawa, Y. Kagawa, and M. Kohyama, *Surf. Sci.* **542**, 45 (2003).
- <sup>51</sup>S. V. Dmitriev, N. Yoshikawa, M. Kohyama, S. Tanaka, R. Yang, and Y. Kagawa, *Acta Mater.* **52**, 1959 (2004).
- <sup>52</sup>S. V. Dmitriev, N. Yoshikawa, M. Kohyama, S. Tanaka, R. Yang, Y. Tanaka, and Y. Kagawa, *Comput. Mater. Sci.* **36**, 281 (2006).